Surfaces and Interfaces 68 (2025) 106586

Contents lists available at ScienceDirect

Surfaces and Interfaces

journal homepage: www.sciencedirect.com/journal/surfaces-and-interfaces

Segregation-driven formation of bismuth quantum dots in parabolic GaAsBi/AlGaAs quantum structures

Augustas Vaitkevičius [a,b,*], Aivaras Špokas [a,b], Andrea Zelioli [a], Ugnė Cibulskaitė [b], Andrius Bičiūnas [a], Evelina Dudutienė [a], Bronislovas Čechavičius [a], Martynas Skapas [a], Aurimas Čerškus [a], Martynas Talaikis [a], Piotr Baranowski [c], Piotr Wojnar [c], Renata Butkutė [a,b]

[a] Center for Physical Sciences and Technology, Saulėtekio av. 3, Vilnius, LT-10257, Lithuania
[b] Vilnius University, Faculty of Physics, Institute of Photonics and Nanotechnology, Saulėtekio av. 3, Vilnius, LT-10257, Lithuania
[c] Institute of Physics, Polish Academy of Sciences, Aleja Lotników 32/46, Warsaw, PL-02-668, Poland

ARTICLE INFO

Keywords:
Molecular beam epitaxy
Quantum wells
Parabolic barriers
Quantum dots
Bismuth
Segregation
High resolution transmission electron microscopy
Luminescence

ABSTRACT

This work is focused to investigation of bismuth quantum dots formation mechanism using segregation process via two types of annealing of gallium arsenide bismide quantum well structures with aluminium gallium arsenide parabolic barriers: *in-situ* annealing in a molecular beam epitaxy reactor immediately after growth and *ex-situ* in a rapid thermal annealing oven. Both processes were performed in the range of temperatures of 600–750 °C and adjusting annealing time from 0 to 180 s. The structures were characterized using high resolution transmission electron microscopy, temperature and time dependent photoluminescence measurements, cathodoluminescence, Raman spectroscopy, and dimensional analysis. Transmission electron microscopy images demonstrated that *in-situ* annealing in a reactor at temperatures up to 750 °C for 0–150 s results in the formation of randomly oriented Bi quantum dots with a dominant size of about 10–15 nm, exhibiting cathodoluminescence at 0.9 eV at 10 K. The investigation using *ex-situ* rapid thermal annealing showed a trend that with increase of annealing temperature the intensity of quantum well related emission reduces, peak is redshifted and broadens, while the quantum dot related emission increases in intensity, suggesting the diffusion of bismuth atoms from the bismide lattice leading to formation of pure bismuth quantum dots.

1. Introduction

The engineering of new materials functioning in the near infrared (NIR) spectrum region has attracted a lot of attention of the scientific community in the last decade due to possible applications in sensing systems. Fundamental knowledge allows material engineering specialists to manipulate properties of semiconducting materials and parameters of devices. Moreover, various techniques and technological protocols of well-known fundamental processes, for example, the modification of epitaxy methods by inserting interruptions for enhancement of atom diffusion, carrying out *ex-situ* and *in-situ* thermal annealing to smooth out the boundaries of layers open the possibility to control the size, density of nanostructures and smoothness of interfaces.

One example of such engineering is GaAsBi, a compound that belongs to the family of bismides, discovered two decades ago. It was shown that bismides are promising compounds due to the NIR range emission range, achievable by partially replacing As atoms by Bi atoms in the GaAs lattice. The reduction of the GaAsBi energy bandgap is much more efficient in comparison to well-known classical compounds, such as InGaAs, etc. It is proven, that 1% of Bi can reduce the energy bandgap up to 88 meV [1–3]. Increasing Bi content in GaAs from 0 to 11–14% GaAsBi compound energy bandgap can be changed from 1.42 to 0.75 eV [4], which corresponds to spectral range from 875 to 1500 nm. Furthermore, GaAsBi as a compound shows very low energy bandgap dependence on temperature, what means, that bismide-alloy-based devices could work at room temperature without additional cooling. Despite intensive investigations of bismides and few publications on NIR emitters [5–9] , their application is held-back by technological challenges. The low epitaxy temperature and As/Ga ratio close to 1 both lead to poor crystallinity and weak luminescence [10,11]. Moreover, bismuth tends to segregate to the surface at high temperatures standard to GaAs epitaxy initiating the

* Corresponding author at: Center for Physical Sciences and Technology, Saulėtekio av. 3, Vilnius, LT-10257, Lithuania.
E-mail address: augustas.vaitkevicius@ftmc.lt (A. Vaitkevičius).

https://doi.org/10.1016/j.surfin.2025.106586
Received 7 March 2025; Received in revised form 11 April 2025; Accepted 27 April 2025
Available online 13 May 2025

formation of droplets at the interfaces and on the cap layers. Due to a very narrow As/Ga technological window and very low bismuth solubility at low temperature these droplets often consist of Ga and Bi phases [11–13]. It was shown that the crystallinity of GaAsBi layers can be improved and bismuth surplus reduced by growing under arsenic-rich conditions and performing thermal post-deposition processes at temperatures higher than 450 °C [14–17]. On the other hand, annealing at higher temperatures, results in a reduction of photoluminescence (PL) [18,19]. Moreover this annealing leads to a reduction of Bi content in the lattice and to the appearance of nanometre-size clusters [17]. Similar studies on Ge nanoparticles demonstrated crystallinity, spherical shape and homogeneous distribution of single phase nanoparticles that have a tunable size and incorporation of Mg in Ge matrix [20]. Also, after annealing a phase separation in the binary nanoparticle structure has been reported; the resulting nanocrystals typically consist of pure rhombohedral bismuth and separate zinc blende Bi-rich GaAsBi phases with nanocrystal size varying from 5 to 20 nm [21,22].

Our previous *ex-situ* annealing of 1.5 μm-thick GaAsBi layers and GaAsBi/GaAs quantum wells has uncovered several important features: intense PL in the range of 1.35–1.5 μm and damage of the QW structure due to bismuth segregation to the sample surface. It was demonstrated that high-temperature annealing of GaAsBi with a large Bi content (more than 6%) leads to the appearance of nanometre-size pure Bi crystals [23–25]. In Ref. [24] theoretical prediction demonstrates that bismuth nanocrystals with size less than 60 nm become semiconductors with an indirect bandgap, while reduction of their diameter below 16 nm results in the formation of a semiconductor with a direct bandgap, enabling non-equilibrium carriers to recombine radiatively. To understand bismuth segregation and agglomeration to quantum dots several techniques, such as transmission electron microscopy (TEM), scanning electron microscopy (SEM) and atomic force microscopy (AFM) were used. The obtained results demonstrated the influence of post-annealing on Bi agglomeration into spherical nanoclusters of various diameters in thick GaAsBi layers. While segregation of Bi atoms to the surface distorts GaAsBi/GaAs MQW structures and only the first QW near the substrate is left containing Bi dots. These results led to investigating epitaxy processes with bismuth blocking layers. The idea to use 20 nm-thick AlAs layer as a blocking layer was studied in Ref. [26] where Ge substrate atom interdiffusion to GaAs is stopped. The studies of *ex-situ* annealing of structures containing GaAsBi MQWs surrounded by AlAs barriers revealed the formation of Bi nanoparticles at temperatures higher than 750 °C. TEM images showed that AlAs barriers blocked Bi segregation to the surface and enabled bismuth nanoclusters diameter control [24]. The study of annealing of GaAsBi MQWs with AlAs barriers not only showed successful Bi nanoparticles size control by QW width, but also demonstrated luminescence from QDs in the range of 1000–1300 nm [24,27]. The results of optical measurements supported the findings on bismuth nanocolloidal particles [28].

The main goal of this work was to explore the formation mechanism of Bi QDs using the process of segregation as an alternative to the Stranski–Krastanov (S–K) method, based on deposition of a compressively strained layer with larger lattice constant on lower lattice constant material [29–31]. It is important to highlight that Bi QDs formation has yet to be successfully realized via S–K growth mechanism. To achieve this goal different growth protocols and thermal processes using *in-situ* post-deposition annealing in a MBE reactor and *ex-situ* annealing in a rapid thermal annealing (RTA) oven under arsenic overpressure conditions were carried out. The focus was set on the annealing temperature and time. The structure of interest in this work was GaAsBi MQW structures with AlGaAs parabolic barriers. By implementing this study, it was expected to verify the ability to use AlGaAs grading (with only up to 30% Al) barrier instead AlAs, first, for the optimum quantum confinement, and second, to examine the effectivity of bismuth blocking. HR-TEM and Raman spectroscopy were used for study of the influence of temperature and time on segregation of bismuth atoms. Various spectroscopy measurements — temperature and time dependent photoluminescence, cathodoluminescence and dimensional analysis, were performed to prove the quantum confinement in Bi nanocrystals.

The results are intended to serve as proof of concept, demonstrating that segregation processes can be effectively utilized for the formation of Bi QDs and applied in the active regions of photonics devices.

2. Methods

2.1. Sample preparation

The study was performed on GaAsBi QW structures grown using MBE, and *in-situ* annealed directly after growth. In order to explore different scenarios of bismuth blocking two types of samples A and B were designed and grown. Each structure contained two 10 nm-thick GaAsBi QW grown under Bi-rich conditions to introduce large content of bismuth (more than 10–12%; to obtain the critical mass to form Bi QDs in the QW). For detailed investigation of crystalline quality impact on Bi QDs formation, the main technological parameters, As to Ga flux ratio and growth temperature, varied from 0.8 to 1.1 and 400–425 °C, respectively (see Table 1).

The quantum wells in structures A and B were inserted between symmetric parabolic AlGaAs barriers. In sample B quantum wells were additionally surrounded by ultrathin (up to 1 nm) tunnelling AlAs barriers.

In both structures the parabolic barrier profiles were grown by changing the Al content from 30% at the top of the barrier to pure GaAs at the bottom for both QWs [24]. Higher bonding energy of AlAs in comparison GaAs blocks bismuth diffusion through the AlAs barrier. AlAs barrier is not optimal for the optical properties of the QDs so it is necessary to optimize the composition of the AlGaAs barrier. The parabolic nature of the AlGaAs barrier could allow to understand how much Al content is needed to stop Bi diffusion outside the QW. More details on the technological properties details, defects and optical properties are reported in previous work [32]. Such profile enhances carrier collection into the QW and increases radiative recombination more than fifty times when exciting the structure with energy higher than the barrier. On the other hand, parabolic barrier could provide information about the AlGaAs effectiveness in stopping bismuth atom interdiffusion to the barrier and versatility in controlling the diameter of Bi QDs.

The design with ultra-thin AlAs tunnelling barriers in sample B aims to further suppress bismuth interdiffusion between the well and barrier. Thus, selected designs would be favourable not only for extending knowledge about Bi segregation process in the well and agglomeration to quantum dots but also for optimization of quantum confinement which could enhance optical properties. Moreover, it was expected that the QD diameter would vary with the QW thickness, and that annealing would lead to the formation of Bi QDs of the preferred size. The sketches of both type of structures are presented in Fig. 1.

As-grown structures were annealed in the reactor in the range of 650–750 °C for 0–150 s to form Bi QDs in QW employing the segregation process. The ranges were selected taking into account our previous experiments for Bi QD formation [27]. The 0 s time means that the temperature of as-grown sample was increased up to annealing temperature and then immediately reduced down to 600 °C for the growth of AlGaAs spacer. To define the annealing "window" limited by temperature and time, and segregation process intensity it was decided to perform two cardinally different processes: (i) annealing at lowest temperature of 675 °C for 0 s, (ii) annealing at highest temperatures 730 °C and 750 °C for 150 s and 110 s respectively. The (ii) case could show the impact of higher temperature/shorter time and lower temperature/longer time.

Three samples were grown on semi-insulating GaAs substrates, two more structures were grown using conducting *n*-type GaAs substrates

Table 1
Main growth parameters of structures investigated in this work.

Sample	As/Ga ratio	Bi/Ga ratio	d_{AlAs}, nm	Growth T, °C	Annealing T, °C	Annealing time, s
A730	0.881	0.802	0	400	730	150
A675	1.011	1.164	0	425	675	0
B750	1.011	1.164	0.9	425	750	120
C600	0.966	0.597	0	350	600	0
C700	0.958	0.597	0	350	700	180

(Samples C) to compare the influence of temperature on the segregation process, due to the higher thermal conductivity of doped GaAs substrates [33]. It is important to point out, that the growth and annealing temperatures differed about 50 °C compared to semi-insulating GaAs substrates, thus MQW structures were grown and annealed at lower temperatures.

The main growth parameters of investigated structures are presented in Table 1. The samples were named by A, B and C capital letters depending on the substrate used (semi-insulating A and B or conducting C) and barrier design (sample A and C with simply parabolic barriers, sample B - with double barriers: parabolic and tunnelling). The number next to letter indicates the annealing temperature.

To compare the effect of annealing in reactor and oven, some *in-situ* heated samples were additionally annealed in RTA at 700 °C and 750 °C for 180 s. As/Ga ratio and Bi/Ga ratio present the beam equivalent pressure ratios for As and Ga and Bi and Ga used for the growth of GaAsBi QW; d_{AlAs} – thickness of AlAs tunnelling barrier; growth T – temperature of bismide QW growth, annealing T – temperature of *in-situ* annealing in the reactor; annealing time — time of *in-situ* annealing in the reactor; 0 annealing time means that the temperature of as-grown sample was increase up to annealing temperature and then immediately reduced down to 600 °C for the growth of AlGaAs spacer. To mimic the process the temperature in both cases was measured by thermocouple and temperature increase and decrease profiles were set keeping the same ramp rate of 50 °C/min.

2.2. Characterization techniques

The structural high-resolution measurements of nanoparticles were carried out by FEI Tecnai G2 F20 X-TWIN TEM with STEM module, equipped with an X-ray energy-dispersive spectroscopy (EDS) detector for elemental mapping and a high-angle annular dark-field (HAADF) detector for *Z*-contrast imaging. FEI Helios Nanolab 650 dual beam microscope equipped with an Omniprobe manipulator was used to prepare specimens for the TEM measurements. The lamellas from each sample were cut with focused gallium ion source for HR-TEM characterization and analysis.

The Raman spectra were recorded in the backscattering geometry using inVia Raman microscope (Renishaw, Wotton-under-Edge, UK) equipped with a thermoelectrically cooled (−70 °C) CCD camera. A 532 nm diode-pumped solid-state laser served as the excitation source with 0.2 mW of laser power at the sample. The 50× /0.75 NA objective lens and 1800 lines/mm grating were employed for spectral acquisition, with a total accumulation time of 40 min. The Raman frequencies were calibrated using the 520.7 cm^{-1} band of a silicon standard. Vibrational mode parameters were determined by fitting the spectra with Gaussian–Lorentzian components using GRAMS/A1 8.0 software (Thermo Scientific).

A continuous-wave DPSS laser (MGL-III-532, CNI) with a wavelength of 532 nm and an average power of 400 mW, producing a laser spot diameter of 0.2 mm, was used as the excitation source for temperature-dependent (TD) PL measurements. The PL signal was detected using a liquid nitrogen-cooled InGaAs photodetector (IGA2.2-010-LN, EOS).

The spatial distribution of PL characteristics was analysed by measuring confocal microphotoluminescence (μPL) at sub-micrometre scale

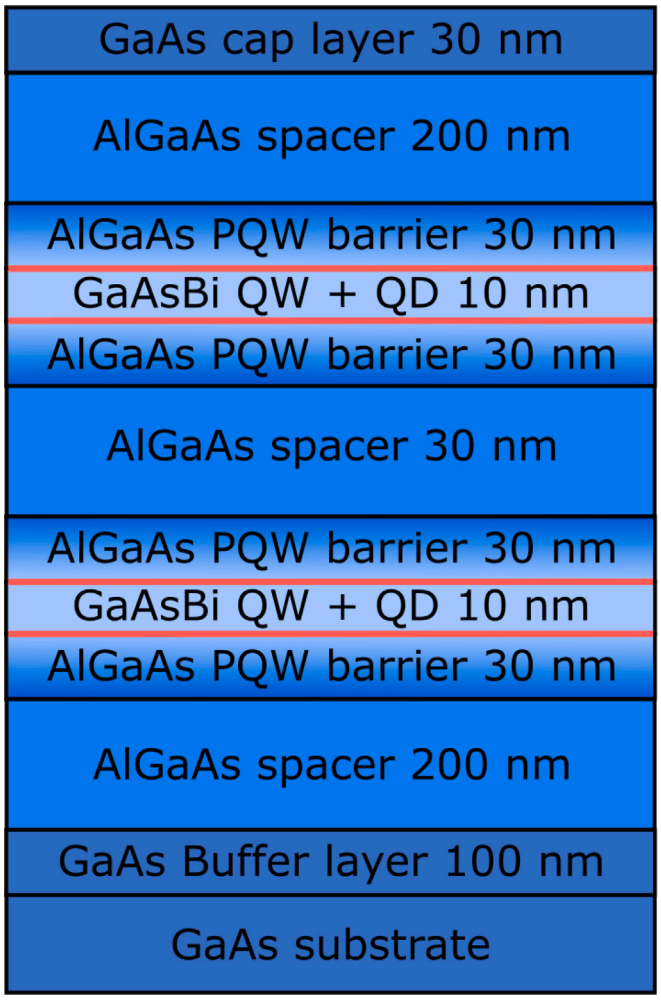

Fig. 1. The schematic view of the structure demonstrating 2× GaAsBi QW with parabolic profile AlGaAs barriers. Tunnelling barriers enveloping the two GaAsBi QWs are pictured in red and only present in sample B750.

using a WITec Alpha 300S microscope in confocal mode. A 662 nm laser diode (Integrated Optics) was employed for excitation, and a high numerical aperture objective lens (NA = 0.8) provided submicrometer spatial resolution. For spectrally resolved measurements, the confocal microscope was connected via optical fibre to an Andor spectrometer, which was paired with a thermoelectrically cooled InGaAs CCD camera capable of detecting PL signals in the NIR region.

CL measurements were conducted with the samples placed on a liquid helium cryostage (Kammrath and Weiss) within a Zeiss Evo HD 15 SEM, where the temperature is kept stable at 10 K. The CL signal was collected by a parabolic mirror and directed to the Horiba Jobin Yvon's CLUE detection system.

The continuous wave (CW) PL and time-resolved (TR) PL spectra were measured using a standard setup with a fully automated 1 m focal length monochromator (FHR1000, HORIBA Jobin Yvon Inc.), achieving the spectral dispersion of 0.8 nm/mm. The sample was mounted in a closed-cycle helium optical cryostat (SHI-4, Janis Research Company) and its temperature was changed from room temperature to 4 K. An Ar-ion laser (131 LGA, LG-Laser Technologies GmbH) with excitation energy in the range of 2.2–2.4 eV was used for excitation in CW-PL measurements and a pulsed 531 nm DPSS microchip laser (STA-01 SH-1, Standa Ltd.) with a pulse full width at half maximum (FWHM) of 400 ps and repetition rate of 10 kHz was used as an excitation source in TR-PL measurement. The signal was detected by an infrared single

photon detector based on an InGaAs/InP avalanche photodiode (ID230, ID Quantique) being thermoelectrically cooled and operating in the photon counting regime. The PL spectrum was registered with a gated photon counter/multiscaler (PMS-400 A, Becker & Hickl GmbH). The TR-PL decay curves were measured with the time-correlated single-photon counting system (SPC-130, Becker & Hickl GmbH). The results were fitted by the multiexponential function $I_{PL}(t) = \sum A_i e^{-\frac{t}{\tau_i}}$, and the average decay times were calculated as $\tau_{av} = \frac{\sum A_i \tau_i^2}{\sum A_i \tau_i}$.

3. Results and discussion

3.1. HR-TEM measurements

Visually from the HR-TEM pictures is clearly seen that quantum dots of various size have been formed in all samples (see Fig. 2(a–h) except sample A675 (see Fig. 2i).

HR-TEM images zoomed in on individual QDs (see Fig. 2b,d,e,h) also demonstrate pure bismuth, and do not evidence any gallium phase and no structural defects in the QDs and on the boundary of the QDs, the cross-section images also evidence that the QDs in the well are oriented randomly.

Linking the sample growth and *in-situ* annealing condition on the Table 1 and HR-TEM images, several trends can be observed. First, no intensive Bi atoms segregation and agglomeration to QDs is visual for the sample A675. This sample was grown supplying high As and Bi (much higher than optimal) fluxes. Due to arsenic priority to bond with Ga atoms, only few percent of Bi incorporate to the lattice. Fast annealing at low temperature only improves the crystalline structure. Second, with increase of temperature and time (sample A730) intensive bismuth atoms segregation and QDs formation is seen. The Bi segregation tracks visible in the picture allow to suppose that the temperature and time are not high enough to completely aggregate bismuth surplus to the QDs. Due to higher thermal conductivity of conducting GaAs substrate, distinguished segregation tracks and QDs were recorded for sample C600 at lower temperature. Third, the HR-TEM cross-section picture of sample C700, annealed at highest 700 °C temperature and for the longest time of 180 s, demonstrate no tracks and highest density of Bi QDs. Additionally, the density of QDs in the samples grown on semi-insulating substrate supplying very high As flux (even for high Bi flux during the growth) is very low. It could be explained by too small bismuth content in GaAsBi QW, meaning that bismuth surplus completely segregates and agglomerates to QDs (see Fig. 2d). Moreover, from Fig. 2d it can be deduced that only 1 nm thick AlAs tunnelling barrier can effectively suppress Bi diffusion to the parabolic barrier, and in such way limit Bi QDs height.

3.2. Evaluation of density of quantum dots

The definition of QDs in semiconducting structures can be applied only for characteristic density of nanoparticles. It is well known that the typical QD density for self-assembled QD arrays reaches the concentration around 3×10^{11} cm^{-2}. On the other hand, it was demonstrated that by applying the strain-compensated S–K method, InAs QDs grown on an InP substrate exhibit a much higher density of about 2×10^{13} cm^{-2} [34].

The statistical analysis of QDs in the QW were done to estimate the density of QDs in the QW and to justify that QD density requirement is fulfilled. The QD density statistics were obtained from three lamellas of each sample. The distribution was analysed and compared in both QWs as well as in samples grown on semi-insulating and conductive GaAs substrates. Comparing TEM images of samples grown on different substrate one more tendency was observed: the slightly higher QDs density was agglomerated in the samples grown on semi-insulating GaAs (see Table 2). Table 2 also presents the detailed information about QDs density in first and the second quantum well. Possibly the higher density of quantum dots in the first well of sample A730, grown on semi-insulating substrate, can be justified by small temperature difference between first and second QW.

Table 2
Bi QDs density statistics of three samples.

Sample	QDs density first QW, cm^{-2}	QDs density second QW, cm^{-2}
A730	7.57E+10	6.23E+10
C600	4.74E+10	3.10E+10
C700	3.54E+10	4.90E+10

3.3. Quantum dot diameter distribution

Further investigation was done to find out the distribution of quantum dot sizes and relation with temperature and annealing time. As mentioned in previous work Bi quantum dot size depends on the width of the GaAsBi quantum well [24]. In these three samples thicknesses of GaAsBi quantum wells were around 20 nm and the distribution shows that the majority of quantum dots form up to 20 nm in diameter. In Fig. 3 the distribution of QD sizes is presented. Based on our previous investigations [24] quantum dots with diameter larger than 16 nm are not taken into account in the statistical analysis, because they exhibit an indirect bandgap.

Fig. 3 demonstrates the size of QDs predominantly falls within the 10 to 15 nm size range. Comparing size distribution of quantum dots in first and second quantum well a slight difference can be seen: the dominating size in second QW is few nanometres smaller than that in the first QW (Fig. 4).

All analysed HR-TEM pictures showed a similar, wide quantum dot size distribution as well as random orientation of QDs in the well. A way for controlling quantum dot sizes could be adopted from previous technological experiments by introducing AlAs barriers to the structure, which already proved to be effective (Fig. 2c–d). The growth and annealing of QW with 1 nm thick AlAs blocking layers confirmed the concept of controlling size and orientation of Bi QDs using the segregation process. This is evidenced in HR-TEM picture of B750 sample (Fig. 2c,d). In which all of the components of the layered structure are visible starting from GaAs buffer layer on the bottom, parabolic barrier with a graded Al content, 1 nm thick AlAs blocking layers (black lines) and bright QWs. The brighter discs in the well are attributed to Bi QDs. When zoomed in, crystalline structure of the QDs is visible (Fig. 2d). The disc shape of some QDs is caused the by blocking layers. The small number of QDs in the first well requires further investigation and optimization of annealing conditions for such type of MQWs.

3.4. Raman measurements

The Raman spectrum of an *in-situ* annealed GaAsBi/AlGaAs QW sample is presented in Fig. 5. A doublet at 269 and 290 cm^{-1} corresponds to the GaAs-like transverse optical (TO) and longitudinal optical (LO) phonon modes, respectively [35–37]. In the backscattering geometry, the TO band is symmetry-forbidden in an ideal GaAs crystal [36,37], but the disorder introduced by Bi disrupts the crystalline lattice symmetry of GaAs, thereby activating the TO mode. The broad and overlapped vibrational modes near 168, 196 and 238 cm^{-1} can be attributed to GaBi-like vibrational modes [37,38]. A weak feature below 100 cm^{-1} could be associated with the withdrawal of bismuth from the GaAsBi lattice and its aggregation to Bi QD [39].

3.5. Photoluminescence measurements

Fig. 6 presents the temperature-dependent PL spectra of an *in-situ* annealed sample (A730), measured over the temperature range of 3–300 K. The PL spectra across the entire temperature range exhibit a single broad PL band (FWHM between 113 meV and 143 meV), with intensity maxima around 1.08 eV at room temperature. Notably, the PL peak position shows minimal variation with temperature, with Varshni

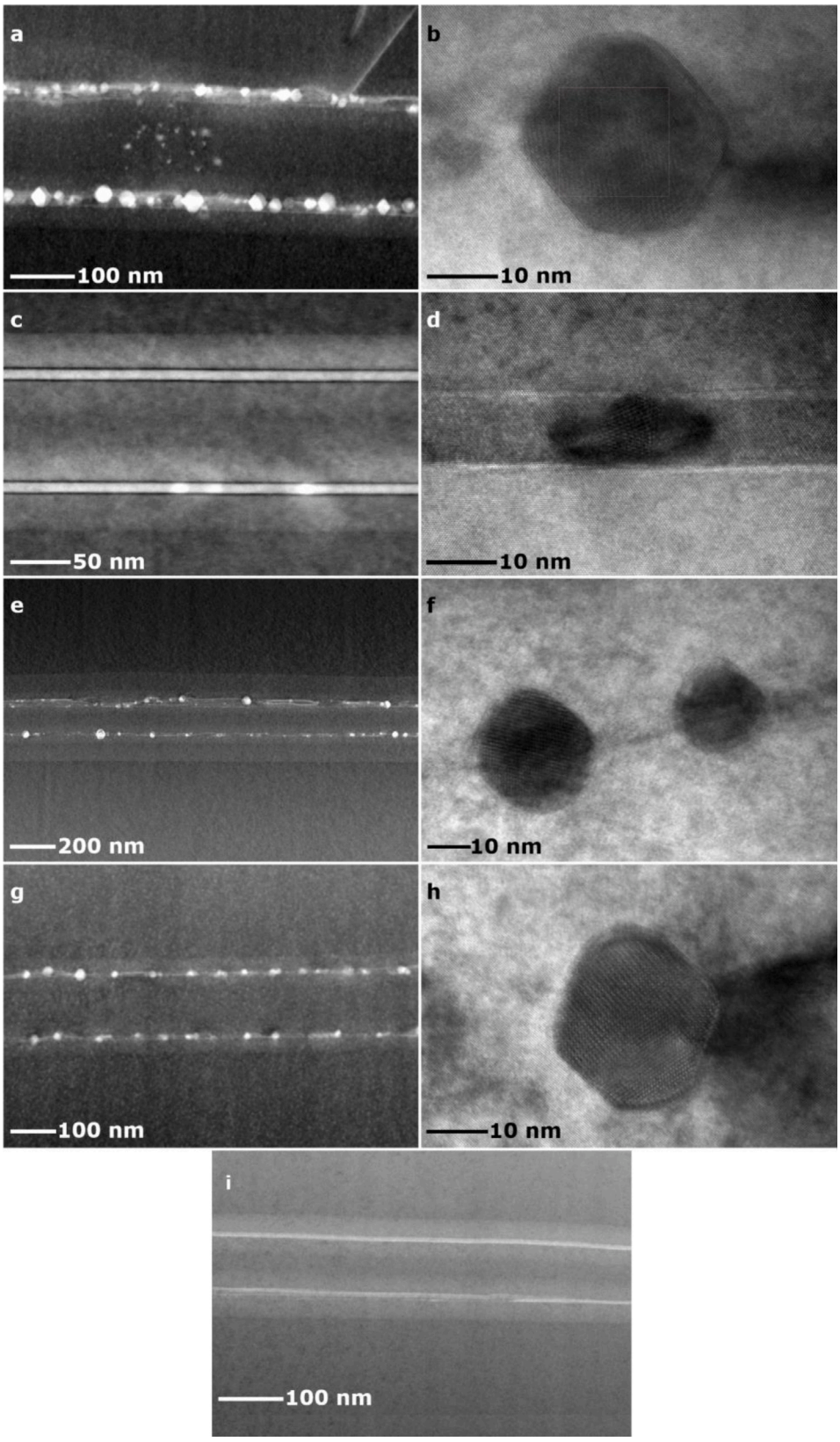

Fig. 2. TEM pictures of samples as-grown and directly annealed at various temperatures and for different time in MBE reactor: sample A730 annealed at 730 °C for 150 s (a, b), sample B750 annealed at 750 °C for 120 s (c, d), sample C600 annealed at 600 °C for 0 s (e, f), sample C700 annealed at 700 °C for 180 s (g, h), sample A675 annealed at 675 °C for 0 s (i). Zoomed in pictures of the respective sample presented in b, d, f, h.

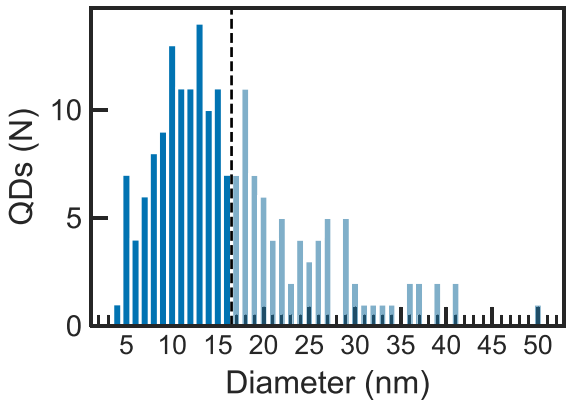

Fig. 3. Cumulative distribution QDs diameter in investigated (Table 2) samples. Dotted line at 16 nm separates direct and indirect band gap QDs.

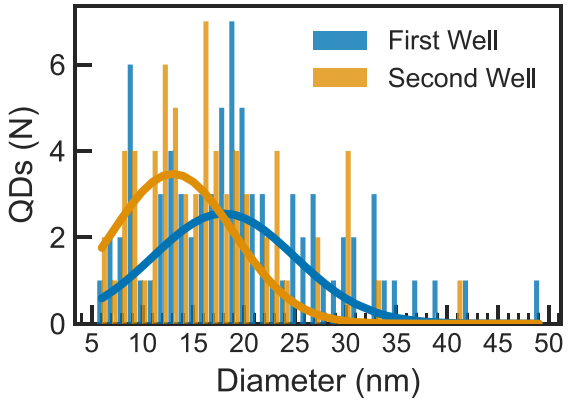

Fig. 4. QDs diameter distribution compared between first and second well. A Gaussian distribution is presented as a guide to the eye.

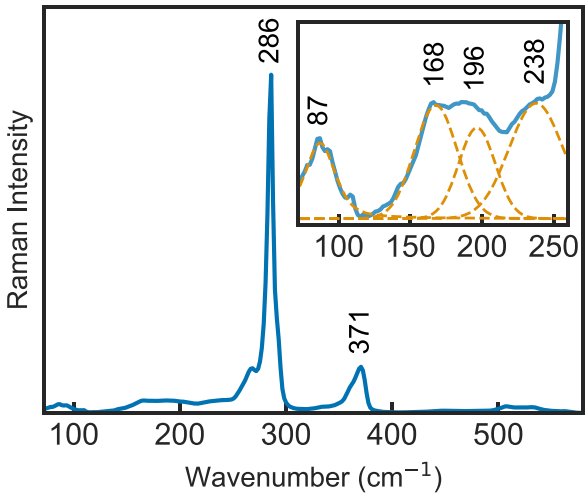

Fig. 5. The Raman spectrum of an *in-situ* annealed GaAsBi/AlGaAs QW sample (A730). The inset highlights the deconvolution of peaks in the low wavenumber region (70–260 cm^{-1}), showing individual components (dashed blue lines) contributing to the overall spectrum (solid purple line).

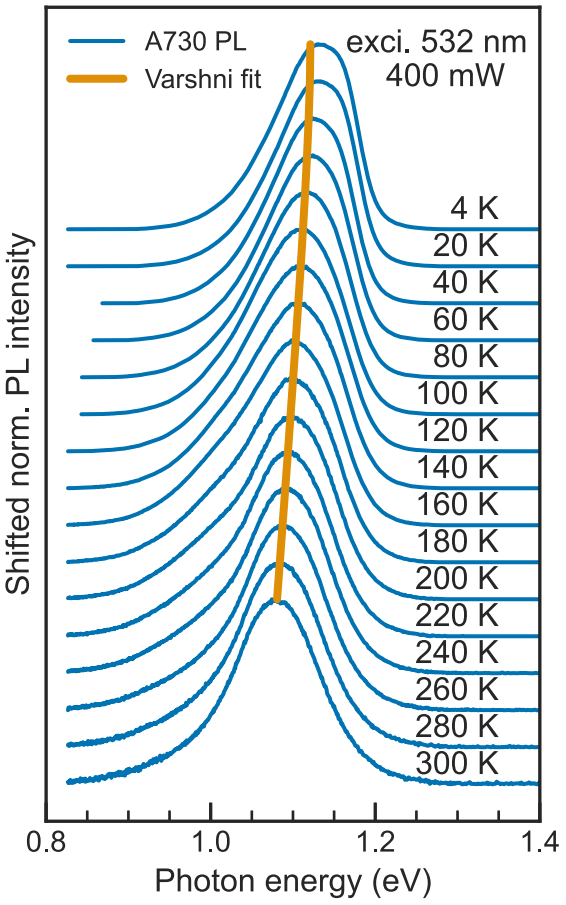

Fig. 6. Temperature-dependent PL spectra of sample A730. The PL spectra are normalized and vertically shifted for clarity, with the red curve representing the Varshni fit [41].

parameters: E(0 K) = 1.121 eV, α = 0.18 meV/K, and β = 100 K, which are consistent with previously reported Varshni parameters for Bi QDs [24]. Additionally, the temperature dependence of the PL spectra for the *in-situ* annealed sample A730 differs from the behaviour observed in a similar, but unannealed, GaAsBi double PQW structure [40], where the PL peak position varied significantly with temperature. This suggests that the observed PL signal from the *in-situ* annealed sample is more likely related to emission from Bi QDs than from the GaAsBi QW. However, this supposition requires further investigation using different optical methods.

3.6. Microphotoluminescence measurements

μPL mapping was conducted for samples A675, A730, and B750, targeting two distinct energy ranges, 1.4–1.5 eV and 0.9–1.3 eV, corresponding to characteristic emissions from GaAs and GaAsBi structures, respectively. The maps reveal inhomogeneous intensity distributions across both energy ranges, indicating non-uniformity (summarized in Table 3) on the micro scale that can be caused by bismuth segregation, variations in quantum well structure and presence of defects.

Fig. 7 presents μPL maps for sample A730 after RTA at 750 °C. Analogous maps were acquired for all samples under study to assess emission homogeneity. The homogeneity was quantified by calculating the standard deviation (SD) of PL integrated intensity across each map. Additionally, the Pearson correlation coefficient (PCC) was computed between the maps of intensity across different energy ranges to evaluate

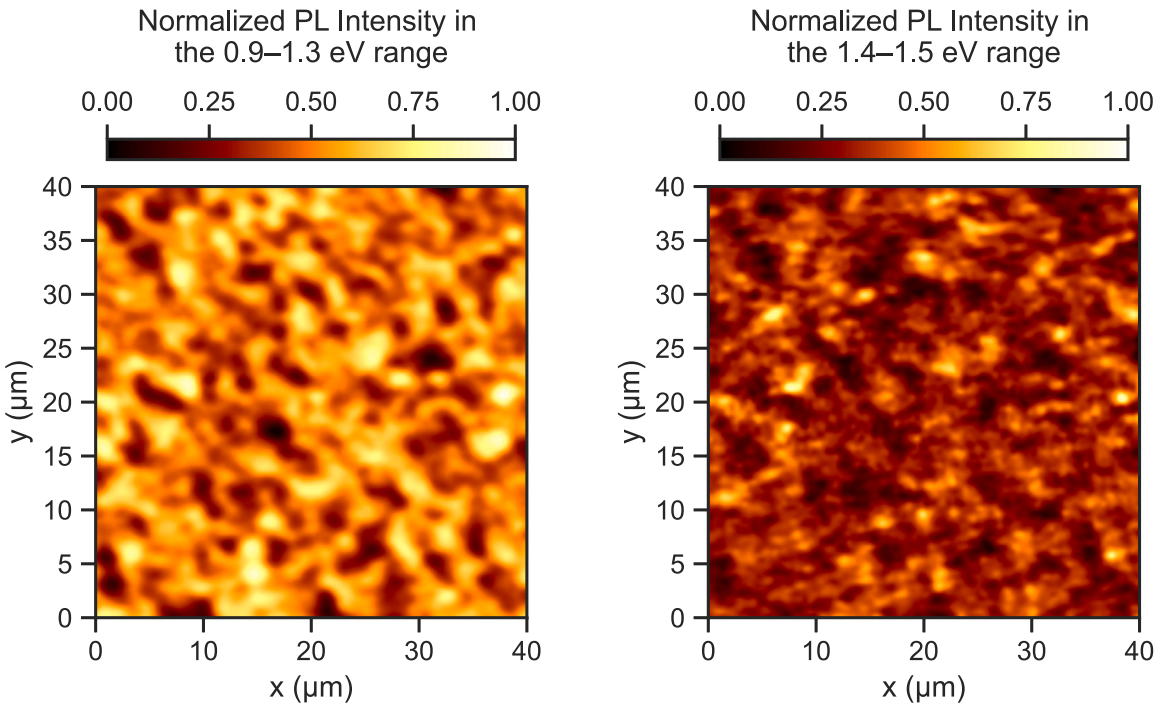

Fig. 7. Spatial distribution of PL intensity measured for sample A730 after RTA at 750 °C. Left: PL intensity map in the 0.9–1.3 eV range, corresponding to GaAsBi emissions. Right: PL intensity map in the 1.4–1.5 eV range, attributed to GaAs emissions.

the degree of spatial correlation between these emission regions. These results are presented in Table 3.

For sample A730, GaAs emission homogeneity improves significantly with RTA, as indicated by a reduction in standard deviation from 52.31% in the as-grown state to 30.9% at 700 °C, and further to 5.4% at 750 °C. This trend suggests that higher annealing temperatures promote more uniform GaAs emission regions. Conversely, GaAsBi emission becomes less homogeneous with increased annealing temperature, as the standard deviation rises from 3.64% in the as-grown state to 5.54% at 700 °C, and markedly to 13.16% at 750 °C, indicating that higher temperatures lead to greater variability in bismuth distribution within the GaAsBi layer.

For sample A675, GaAs emission homogeneity is lowest in the as-grown state with a standard deviation of 22.49%. RTA at 700 °C and 750 °C results in a more uniform distribution, with GaAs SD values stabilizing at 10.54% and 11.24%, respectively. In contrast, GaAsBi emission homogeneity decreases sharply upon annealing at 700 °C, with SD increasing from 8.84% to 30.87%, suggesting substantial disruption in the bismuth distribution. However, at 750 °C, GaAsBi homogeneity partially recovers, with SD dropping to 15.8%, indicating some stabilization in the emission properties at the higher temperature. For sample A675, the GaAs emission follows a similar pattern to A730, with homogeneity improving progressively as the SD decreases from 16.81% in the as-grown state to 15.03% at 700 °C, and further to 11.15% at 750 °C. GaAsBi emission homogeneity also decreases steadily with annealing, with the SD rising from 9.31% as-grown to 12.17% at 700 °C, and to 15.72% at 750 °C, showing a consistent trend of increased spatial variability in the GaAsBi region with higher temperatures.

In sample A730, PCC is negligible in the as-grown (0.063) and 700 °C annealed states (0.006), indicating minimal spatial correlation. However, after annealing at 750 °C, PCC rises to 0.479, suggesting improved spatial alignment. This likely results from defect reduction in the GaAs region, enhancing crystal quality and promoting consistent bismuth segregation in GaAsBi.

Table 3
Summary of standard deviations (SD) in photoluminescence intensities for GaAs and GaAsBi regions, along with Pearson correlation coefficients (PCC) between GaAs and GaAsBi emissions in samples A730, A675, and B750.

Sample	Annealing	GaAs SD (%)	GaAsBi SD (%)	PCC
A730	As grown	52.31	3.64	0.063
	180 s at 700 °C	30.9	5.54	0.006
	180 s at 750 °C	5.4	13.16	0.479
A675	As grown	22.49	8.84	0.504
	180 s at 700 °C	10.54	30.87	0.068
	180 s at 750 °C	11.24	15.8	0.325
B750	As grown	16.81	9.31	0.434
	180 s at 700 °C	15.03	12.17	0.220
	180 s at 750 °C	11.15	15.72	0.481

For A675, PCC starts higher in the as-grown sample (0.504), drops to negligible levels at 700 °C (0.068), and partially recovers to 0.325 at 750 °C, reflecting some realignment as GaAs quality improves. B750 shows a similar trend to A730, with PCC rising from 0.220 at 700 °C to 0.481 at 750 °C, indicating that higher annealing temperatures foster better spatial coherence between GaAs and GaAsBi emissions.

Overall, the data suggest that higher annealing temperatures improve GaAs crystal structure and defect reduction, which enhances the spatial alignment and homogeneity of GaAsBi quantum dot distributions.

3.7. Cathodoluminescence measurements

Cathodoluminescence intensity was measured as a function of energy for samples A675, and B750 under different RTA conditions. Figs. 8 and 9 show the normalized CL spectra, highlight the changes in optical properties and quantum dot formation after annealing at various temperatures.

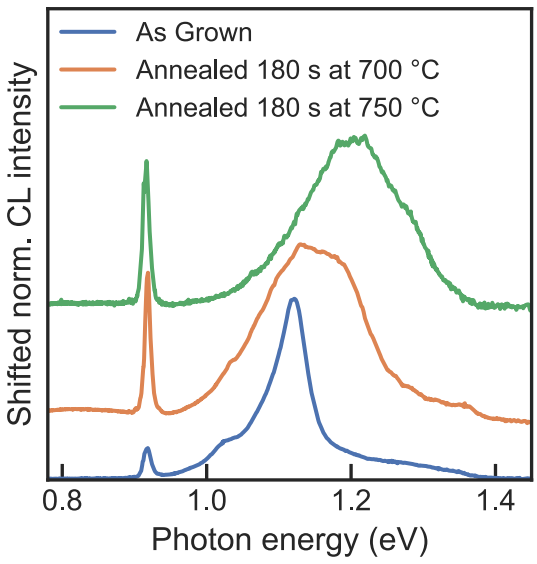

Fig. 8. Sample A675 CL Measured at 10 K. Comparison of As Grown sample with those annealed for 180 s at 700 °C and 750 °C.

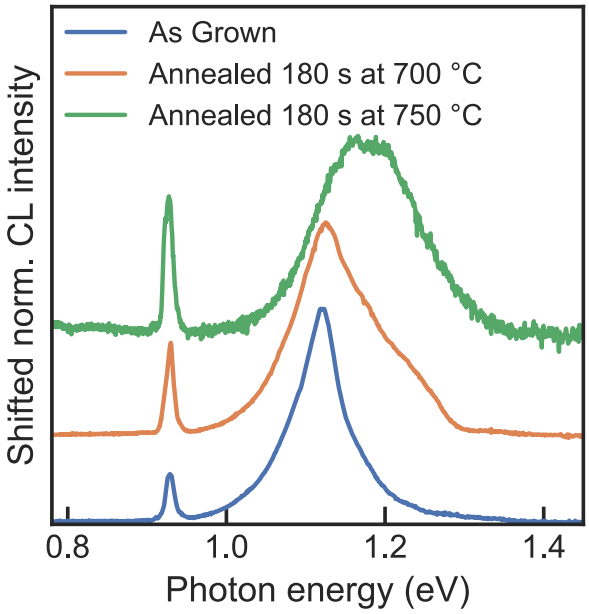

Fig. 9. Sample B750 CL Measured at 10 K. Comparison of As Grown sample with those annealed for 180 s at 700 °C and 750 °C.

In Fig. 8, depicting the CL spectra for sample A675. The as grown sample already shows a narrow CL band around 0.91 eV and a more pronounced peak around 1.11 eV, suggesting that QDs are present even without RTA. Upon RTA at 700 °C, the CL intensity of the line around 0.91 eV increases, and the peak becomes more defined, while the broader peak at approximately 1.2 eV becomes wider and the mean emission energy undergoes a redshift. When the annealing temperature is raised to 750 °C, a significant shift of wider, higher energy band is observed. This indicates a decrease of bismuth content inside the quantum well. However, the relatively constant emission energy of the 0.91 eV band indicates a high level of consistency in QD size.

Sample B750 (Fig. 9), exhibits similar trends to the previous samples. In the as grown state, the sample shows a distinct peak near 1.1 eV and another smaller peak around 0.9 eV, which suggests some initial quantum dot formation. After annealing at 700 °C, the CL intensity around 0.9 eV increases, and the broader emission peak at 1.2 eV becomes more pronounced, indicating an improvement in quantum dot formation. When annealed further at 750 °C, the relative CL intensity of the QD band increases, with a dominant peak at approximately 0.9 eV and broader emission extending towards higher energies (1.2 eV). This indicates that the higher annealing temperature enhances the segregation of bismuth into quantum dots, thereby resulting in higher QD luminescence intensity.

Fig. 10 presents spatial maps of CL measurements that offer some insights into the uniformity of both CL intensity and emission energy within the sample.

The first image shows the CL intensity distribution over a 10 × 10 μm^2 area, with colour variations indicating different levels of luminescence intensity. The ratio between the mean CL intensity and its standard deviation is approximately 33%, reflecting a significant degree of inhomogeneity across the sample. This variation points to inconsistencies in the density or segregation efficiency of the quantum dots, which affect the uniformity of the optical properties of the sample.

The second image maps the CL emission energy across the same region, with emission energies ranging from 0.919 to 0.927 eV. The mean emission energy is 0.923 eV, with a standard deviation of 1.47 meV, suggesting relatively low but notable variations in emission energy across the sample. The presence of both high and low emission energy regions suggests that the quantum dot sizes and/or composition are not entirely uniform, potentially due to differences in the local growth or annealing conditions.

Furthermore, the PCC between CL intensity and emission energy was found to be −0.65, indicating a moderate negative correlation. This suggests that regions with higher CL intensity tend to exhibit slightly lower emission energy, and vice versa. Such a relationship may indicate that in areas with stronger quantum dot emission, the quantum dots could be larger, thereby reducing the emission energy, larger quantum dots also imply more reduction of Bi content in the surrounding QW leading to a lower defect density. This negative correlation highlights the presence of inhomogeneities in quantum dot properties throughout the sample.

3.8. Dimensional analysis

The radiative recombination time evolves through the zero-, one-, two- and three-dimensional confinement of the free electron–hole pairs with temperature-dependent power order as Ref. [42].

$$\tau_r(T) \sim T^{\frac{d}{2}}. \tag{1}$$

Thus, the dimensionality d can be evaluated by determining the temperature dependence ($\sim T\alpha$). For non-coupled quantum structures power factor α has been determined. $\alpha = 0$ (for 0D quantum dots), $\alpha = 0.5$ (for 1D nanowires), $\alpha = 0.8$ (in quasi-1D quantum rings), $\alpha = 1$ (in 2D quantum wells), and in $\alpha = 1.5$ (for 3D bulk structures). In coupled quantum structures, there can be other intermediate values. The validity of this method has already been reported in [43–46]. In general, the measured photoluminescence decay time τ_{PL} at temperature T is related to the radiative and nonradiative carrier recombination times τ_r(T) and τ_{nr}(T), respectively, or quantum efficiency η(T) by

$$\frac{1}{\tau_{PL}(T)} = \frac{1}{\tau_r(T)} + \frac{1}{\tau_{nr}(T)}, \quad \tau_{PL}(T) = \eta(T)\tau_r(T). \tag{2}$$

Meanwhile, the temperature dependence of the integrated photoluminescence intensity I_{PL}(T) over the whole peak can be expressed as

$$I_{PL}(T) = I_0 \frac{\tau_{PL}(T)}{\tau_r(T)} \tag{3}$$

where I_0 is a normalization factor which depends on the number of photoexcited carriers. As we used the normalized PL intensities I_{PL}(T)/I_{PL}(4 K), from Eqs. (2) and (3) follows that

$$\tau_r(T)\eta(4\,\mathrm{K}) = \frac{\tau_{PL}(T)}{\frac{I_{PL}(T)}{I_{PL}(4\,\mathrm{K})}}. \tag{4}$$

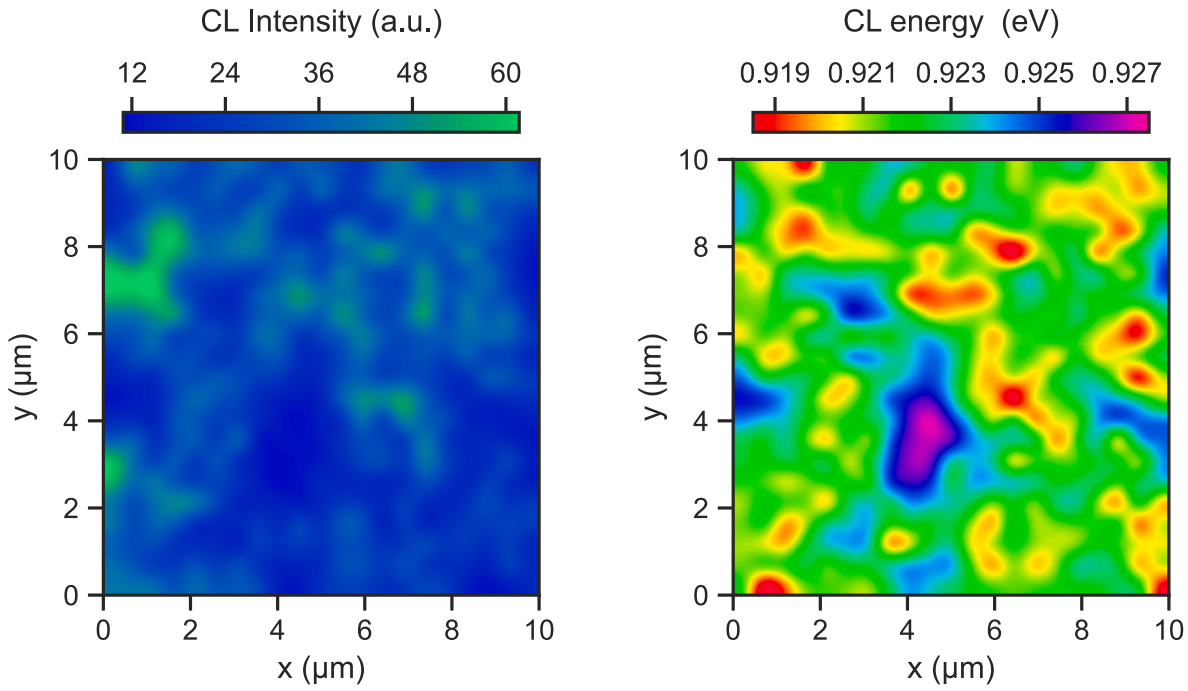

Fig. 10. Spatial maps of cathodoluminescence (CL) measurements for sample A675, highlighting both intensity and emission energy distribution over a 10 μm by 10 μm area.

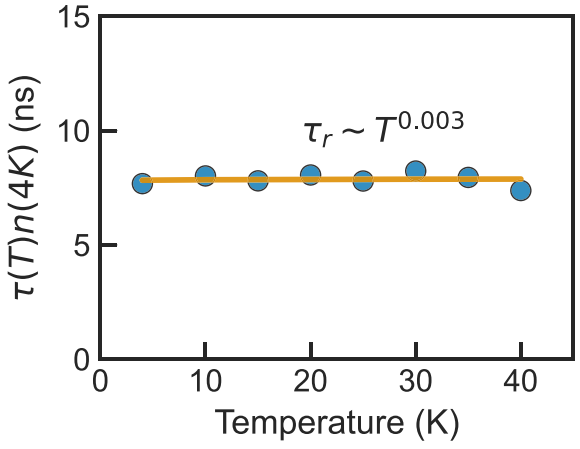

Fig. 11. Radiative recombination times obtained by Eq. (4) amending the PL intensity at 1.1 eV at 4 K. The line is fitting with power function.

Although the quantum efficiency at 4 K is not determined in Eq. (4), the radiative recombination time at various temperatures must be analysed with respect to the power factor in Eq. (4). The power factor is not modified, since quantum efficiency is treated as a scale factor.

This dimensionality analysis has been performed only at low temperatures (below 40 K) where the radiative recombination time can be separated from the whole PL decay time. When nonradiative processes start to dominate, the normalized PL intensity decreases significantly (above 40 K).

The radiative recombination times of this sample were evaluated using Eq. (4) from the average decay times calculated after fitting. The results are shown in Fig. 11. The fitted power factor is ~0. This proves that this emission is related with non-coupled quantum dots.

4. Conclusions

The formation of Bi QDs using *in-situ* segregation process in MBE reactor was studied by HR-TEM cross-section images of MQW samples.

TEM images demonstrated that MBE grown GaAsBi based MQW structures and subsequent *in-situ* annealed at temperatures up to 750 °C for 0–150 s contain randomly oriented Bi QDs with dominating size of about 10–15 nm. Time and temperature are crucial parameters for segregation process, and it must be optimized for different Bi content in GaAsBi QW. Thermal treating time and temperature below the optimum can initiate only partial bismuth agglomeration to QDs with visual bismuth-rich GaAsBi traces in the well.

Statistical analysis of density of Bi QDs formed using segregation revealed the average value of about 6×10^{10} QDs/cm^2, which is close to the values of self-assembled QDs referred in the literature [34].

The AlAs tunnelling barriers proved the successful control of Bi QD size and shape. For reaching of usual QD densities in such type of MQW more detailed study is necessary. The investigation of additional annealing using RTA demonstrated that with increased temperature the intensity of QW related emission is reduced, broadened and redshifted and the QD related emission increases in intensity, suggesting the diffusion and clustering of bismuth atoms.

This technological study will allow the application of this process in the active area of A3-B5-Bi quantum structures of laser diodes or light emitting diodes. We propose two approaches to minimize density of defects related to Bi QDs and surrounding layers, thereby enhancing the efficiency of future devices. For minimization of defects during growth it is possible to implement migration enhanced epitaxy; even at very low temperature very high quality was obtained for AlAs layers [47–50]. Annealing at lower temperatures for a very short time in the growth chamber (*in-situ*) and/or in a RTA oven (*ex-situ*) is also promising. Completion of the preliminary optimization of annealing procedure shown in the manuscript will allows us to avoid bismuth rich tails and increase photoluminescence intensity to a level suitable for applications in lasers. Results presented in this work indicate that the likely conditions for annealing temperature and time are around 700 °C and 180 s, respectively.

In addition, future work must be focused to the complex optical investigations to explore the multiple luminescent channels.

CRediT authorship contribution statement

Augustas Vaitkevičius: Writing – review & editing, Writing – original draft, Visualization, Supervision, Software, Resources, Project

administration, Investigation, Funding acquisition, Data curation. **Aivaras Špokas:** Writing – original draft, Visualization, Methodology, Formal analysis. **Andrea Zelioli:** Writing – original draft, Visualization, Methodology, Formal analysis. **Ugnė Cibulskaitė:** Visualization, Methodology, Investigation. **Andrius Bičiūnas:** Methodology, Investigation. **Evelina Dudutienė:** Writing – original draft, Visualization, Formal analysis. **Bronislovas Čechavičius:** Investigation, Data curation. **Martynas Skapas:** Investigation, Formal analysis. **Aurimas Čerškus:** Writing – original draft, Investigation, Data curation. **Martynas Talaikis:** Formal analysis. **Piotr Baranowski:** Methodology, Investigation. **Piotr Wojnar:** Writing – review & editing, Validation, Supervision, Investigation, Formal analysis. **Renata Butkutė:** Writing – original draft, Validation, Supervision, Resources, Project administration, Funding acquisition, Conceptualization.

Declaration of competing interest

The authors declare the following financial interests/personal relationships which may be considered as potential competing interests: Augustas Vaitkevicius reports financial support was provided by Research Council of Lithuania. If there are other authors, they declare that they have no known competing financial interests or personal relationships that could have appeared to influence the work reported in this paper.

Acknowledgement

This research has received funding from the Research Council of Lithuania (LMTLT), agreement No S-PD-22-7.

Data availability

Data will be made available on request.

References

[1] S. Francoeur, M.-J. Seong, A. Mascarenhas, S. Tixier, M. Adamcyk, T. Tiedje, Band gap of $GaAs_{1-x}Bi_x$, $0 < x \leq 3.6\%$, Appl. Phys. Lett. 82 (22) (2003) 3874–3876, http://dx.doi.org/10.1063/1.1581983.

[2] K. Oe, Characteristics of semiconductor alloy $GaAs_{1-x}Bi_x$, JJAP 41 (Part 1, No. 5A) (2002) 2801–2806, http://dx.doi.org/10.1143/JJAP.41.2801.

[3] V. Pačebutas, K. Bertulis, G. Aleksejenko, A. Krotkus, Molecular-beam-epitaxy grown GaBiAs for terahertz optoelectronic applications, J. Mater. Sci. Mater. Electron. 20 (S1) (2009) 363–366, http://dx.doi.org/10.1007/s10854-008-9625-1.

[4] P. Ludewig, N. Knaub, N. Hossain, S. Reinhard, L. Nattermann, I.P. Marko, S.R. Jin, K. Hild, S. Chatterjee, W. Stolz, S.J. Sweeney, K. Volz, Electrical injection Ga(AsBi)/(AlGa)As single quantum well laser, Appl. Phys. Lett. 102 (24) (2013) 242115, http://dx.doi.org/10.1063/1.4811736.

[5] R. Butkutė, A. Geižutis, V. Pačebutas, B. Čechavičius, V. Bukauskas, R. Kundrotas, P. Ludewig, K. Volz, A. Krotkus, Multi-quantum well Ga(AsBi)/GaAs laser diodes with more than 6% of bismuth, Electron. Lett. 50 (16) (2014) 1155–1157, http://dx.doi.org/10.1049/el.2014.1741.

[6] J. Liu, W. Pan, X. Wu, C. Cao, Y. Li, X. Chen, Y. Zhang, L. Wang, J. Yan, D. Zhang, Y. Song, J. Shao, S. Wang, Electrically injected GaAsBi/GaAs single quantum well laser diodes, AIP Adv. 7 (11) (2017) 115006, http://dx.doi.org/10.1063/1.4985231.

[7] X. Liu, L. Wang, X. Fang, T. Zhou, G. Xiang, B. Xiang, X. Chen, S. Hark, H. Liang, S. Wang, Z. Zhang, Continuous wave operation of GaAsBi microdisk lasers at room temperature with large wavelengths ranging from 127 to 141 μm, Photonics Res 7 (5) (2019) 508, http://dx.doi.org/10.1364/PRJ.7.000508.

[8] Shumin Wang, Xiaoyan Wu, Juanjuan Liu, Wenwu Pan, Chunfang Cao, Liyao Zhang, Yuxin Song, Yaoyao Li, Electrically pumped GaAsBi laser diodes, in: 2017 19th International Conference on Transparent Optical Networks, ICTON, IEEE, Girona, Spain, 2017, pp. 1–3, http://dx.doi.org/10.1109/ICTON.2017.8024777.

[9] Y. Tominaga, K. Oe, M. Yoshimoto, Low temperature dependence of oscillation wavelength in $GaAs_{1-x}Bi_x$ laser by photo-pumping, Appl. Phys. Express 3 (6) (2010) 062201, http://dx.doi.org/10.1143/APEX.3.062201.

[10] R.D. Richards, F. Bastiman, C.J. Hunter, D.F. Mendes, A.R. Mohmad, J.S. Roberts, J.P. David, Molecular beam epitaxy growth of GaAsBi using As_2 and As_4, J. Cryst. Growth 390 (2014) 120–124, http://dx.doi.org/10.1016/j.jcrysgro.2013.12.008.

[11] J. Puustinen, J. Hilska, M. Guina, Analysis of GaAsBi growth regimes in high resolution with respect to As/Ga ratio using stationary MBE growth, J. Cryst. Growth 511 (2019) 33–41, http://dx.doi.org/10.1016/j.jcrysgro.2019.01.010.

[12] E. Sterzer, N. Knaub, P. Ludewig, R. Straubinger, A. Beyer, K. Volz, Investigation of the microstructure of metallic droplets on Ga(AsBi)/GaAs, J. Cryst. Growth 408 (2014) 71–77, http://dx.doi.org/10.1016/j.jcrysgro.2014.09.006.

[13] G. Vardar, S.W. Paleg, M.V. Warren, M. Kang, S. Jeon, R.S. Goldman, Mechanisms of droplet formation and Bi incorporation during molecular beam epitaxy of GaAsBi, Appl. Phys. Lett. 102 (4) (2013) 042106, http://dx.doi.org/10.1063/1.4789369.

[14] B.O. Alazmi, H.H.H. Althebyani, I. Zaied, H. Fitouri, A. Rebey, Thermal annealing effects on the physical properties of GaAsBi/GaAs/GaAs:Si structure, Jas 9 (2) (2023) 164–175, http://dx.doi.org/10.1007/s43994-022-00023-4.

[15] P.C. Grant, D. Fan, A. Mosleh, S.-Q. Yu, V.G. Dorogan, M.E. Hawkridge, Y.I. Mazur, M. Benamara, G.J. Salamo, S.R. Johnson, Rapid thermal annealing effect on GaAsBi/GaAs single quantum wells grown by molecular beam epitaxy, JVST 32 (2) (2014) 02C119, http://dx.doi.org/10.1116/1.4868110.

[16] B. Čechavičius, R. Adomavičius, A. Koroliov, A. Krotkus, Thermal annealing effect on photoexcited carrier dynamics in $GaBi_xAs_{1-x}$, Semicond. Sci. Technol. 26 (8) (2011) 085033, http://dx.doi.org/10.1088/0268-1242/26/8/085033.

[17] R. Butkutė, V. Pačebutas, B. Čechavičius, R. Adomavičius, A. Koroliov, A. Krotkus, Thermal annealing effect on the properties of GaBiAs, Phys. Status Solidi C 9 (7) (2012) 1614–1616, http://dx.doi.org/10.1002/pssc.201100700.

[18] A.R. Mohmad, F. Bastiman, C.J. Hunter, R. Richards, S.J. Sweeney, J.S. Ng, J.P.R. David, Effects of rapid thermal annealing on $GaAs_{1-x}Bi_x$ alloys, Appl. Phys. Lett. 101 (1) (2012) 012106, http://dx.doi.org/10.1063/1.4731784.

[19] A.W. Wood, W. Chen, H. Kim, Y. Guan, K. Forghani, A. Anand, T.F. Kuech, L.J. Mawst, S.E. Babcock, Annealing-induced precipitate formation behavior in MOVPE-grown $GaAs_{1-x}Bi_x$ explored by atom probe tomography and HAADF-STEM, Nanotechnology 28 (21) (2017) 215704, http://dx.doi.org/10.1088/1361-6528/aa6cdb.

[20] M. Aouassa, M. Bouabdellaoui, M. Yahyaoui, T. Kallel, T. Ettaghzouti, S.A. Algarni, I.O. Althobaiti, Mn-doped Ge nanoparticles grown on SiO_2 thin films by molecular beam epitaxy for photodetector and solar cell applications, ACS Appl. Electron. Mater. 5 (5) (2023) 2696–2703, http://dx.doi.org/10.1021/acsaelm.3c00162.

[21] M. Wu, E. Luna, J. Puustinen, M. Guina, A. Trampert, Formation and phase transformation of Bi-containing QD-like clusters in annealed GaAsBi, Nanotechnology 25 (20) (2014) 205605, http://dx.doi.org/10.1088/0957-4484/25/20/205605.

[22] S. Flores, D. Reyes, V. Braza, N. Bailey, M. Carr, R. Richards, D. Gonzalez, The effects of growth interruptions in the GaAsBi/InAs/GaAs quantum dots: The emergence of three-phase nanoparticles, Surfaces Interfaces 56 (2025) 105490, http://dx.doi.org/10.1016/j.surfin.2024.105490, URL https://www.sciencedirect.com/science/article/pii/S2468023024016468.

[23] M. Skapas, E. Luna, S. Stanionytė, K. Graser, R. Butkutė, In situ TEM study of size-controlled bi quantum dots in an annealed GaAsBi/AlAs multiple quantum well structure, ACS Omega 10 (10) (2025) 10432–10437, http://dx.doi.org/10.1021/acsomega.4c10631.

[24] R. Butkutė, G. Niaura, E. Pozingytė, B. Čechavičius, A. Selskis, M. Skapas, V. Karpus, A. Krotkus, Bismuth quantum dots in annealed GaAsBi/AlAs quantum wells, Nanoscale Res. Lett. 12 (1) (2017) 436, http://dx.doi.org/10.1186/s11671-017-2205-7.

[25] Y. Li, L. Zang, D.L. Jacobs, J. Zhao, X. Yue, C. Wang, In situ study on atomic mechanism of melting and freezing of single bismuth nanoparticles, Nat. Commun. 8 (1) (2017) 14462.

[26] C.K. Chia, J.R. Dong, D.Z. Chi, A. Sridhara, A.S.W. Wong, M. Suryana, G.K. Dalapati, S.J. Chua, S.J. Lee, Effects of AlAs interfacial layer on material and optical properties of GaAs/Ge(100) epitaxy, Appl. Phys. Lett. 92 (14) (2008) 141905, http://dx.doi.org/10.1063/1.2908042.

[27] R. Butkutė, K. Stašys, V. Pačebutas, B. Čechavičius, R. Kondrotas, A. Geižutis, A. Krotkus, Bismuth quantum dots and strong infrared photoluminescence in migration-enhanced epitaxy grown GaAsBi-based structures, Opt. Quantum Electron. 47 (4) (2015) 873–882, http://dx.doi.org/10.1007/s11082-014-0019-8.

[28] D. Velasco-Arias, I. Zumeta-Dubé, D. Díaz, P. Santiago-Jacinto, V.-F. Ruiz-Ruiz, S.-E. Castillo-Blum, L. Rendón, Stabilization of strong quantum confined colloidal bismuth nanoparticles, one-pot synthesized at room conditions, J. Phys. Chem. C 116 (27) (2012) 14717–14727, http://dx.doi.org/10.1021/jp304170k.

[29] A. Baskaran, P. Smereka, Mechanisms of Stranski-Krastanov growth, J. Appl. Phys. 111 (4) (2012) 044321, http://dx.doi.org/10.1063/1.3679068.

[30] H. Dobbs, D. Vvedensky, A. Zangwill, Theory of quantum dot formation in Stranski-Krastanov systems, Appl. Surf. Sci. 123–124 (1998) 646–652, http://dx.doi.org/10.1016/S0169-4332(97)00460-1.

[31] T. Kaizu, K. Yamaguchi, Facet formation of uniform InAs quantum dots by molecular beam epitaxy, in: 2002 International Microprocesses and Nanotechnology Conference, 2002. Digest of Papers, Japan Soc. Appl. Phys., Tokyo, Japan, 2002, pp. 146–147, http://dx.doi.org/10.1109/IMNC.2002.1178586.

[32] S. Pūkienė, M. Karaliūnas, A. Jasinskas, E. Dudutienė, B. Čechavičius, J. Devenson, R. Butkutė, A. Udal, G. Valušis, Enhancement of photoluminescence of GaAsBi quantum wells by parabolic design of AlGaAs barriers, Nanotechnology 30 (45) (2019) 455001, http://dx.doi.org/10.1088/1361-6528/ab36f3.

[33] M. Prema Rani, R. Saravanan, Influence of silicon and boron doping on the thermal conductivity of N-GaAs single crystals, MSF 671 (2011) 153–163, http://dx.doi.org/10.4028/www.scientific.net/MSF.671.153.

[34] K. Akahane, N. Yamamoto, T. Kawanishi, Fabrication of ultra-high-density InAs quantum dots using the strain-compensation technique, Phys. Status Solidi A 208 (2) (2011) 425–428, http://dx.doi.org/10.1002/pssa.201000432.

[35] F. Sarcan, Ö. Dönmez, K. Kara, A. Erol, E. Akalın, M. Çetin Arıkan, H. Makhloufi, A. Arnoult, C. Fontaine, Bismuth-induced effects on optical, lattice vibrational, and structural properties of bulk GaAsBi alloys, Nanoscale Res. Lett. 9 (1) (2014) 119, http://dx.doi.org/10.1186/1556-276X-9-119.

[36] J.A. Steele, R.A. Lewis, J. Horvat, M.J.B. Nancarrow, M. Henini, D. Fan, Y.I. Mazur, M. Schmidbauer, M.E. Ware, S.-Q. Yu, G.J. Salamo, Surface effects of vapour-liquid-solid driven Bi surface droplets formed during molecular-beam-epitaxy of GaAsBi, Sci. Rep. 6 (1) (2016) 28860, http://dx.doi.org/10.1038/srep28860.

[37] P. Verma, K. Oe, M. Yamada, H. Harima, M. Herms, G. Irmer, Raman studies on $GaAs_{1-x}Bi_x$ and $InAs_{1-x}Bi_x$, J. Appl. Phys. 89 (3) (2001) 1657–1663, http://dx.doi.org/10.1063/1.1336561.

[38] M. Seong, S. Francoeur, S. Yoon, A. Mascarenhas, S. Tixier, M. Adamcyk, T. Tiedje, Bi-induced vibrational modes in GaAsBi, Superlattices Microstruct. 37 (6) (2005) 394–400, http://dx.doi.org/10.1016/j.spmi.2005.02.004.

[39] E. Haro-Poniatowski, M. Jouanne, J.F. Morhange, M. Kanehisa, R. Serna, C.N. Afonso, Size effects investigated by Raman spectroscopy in Bi nanocrystals, Phys. Rev. B Condens. Matter 60 (14) (1999) 10080–10085, http://dx.doi.org/10.1103/PhysRevB.60.10080.

[40] M. Jokubauskaitė, G. Petrusevičius, A. Špokas, B. Čechavičius, E. Dudutienė, R. Butkutė, Effects of parabolic barrier design for multiple GaAsBi/AlGaAs quantum well structures, Lith. J. Phys. 63 (4) (2023) http://dx.doi.org/10.3952/physics.2023.63.4.8.

[41] Y. Varshni, Temperature dependence of the energy gap in semiconductors, Physica 34 (1) (1967) 149–154, http://dx.doi.org/10.1016/0031-8914(67)90062-6.

[42] L.V. Asryan, Spontaneous radiative recombination and nonradiative Auger recombination in quantum-confined heterostructures, Quantum Electron. 35 (12) (2005) 1117–1120, http://dx.doi.org/10.1070/QE2005v035n12ABEH013093.

[43] T. Okuno, H.-W. Ren, M. Sugisaki, K. Nishi, S. Sugou, Y. Masumoto, Temperature dependence of luminescence decay time of InP quantum disks, JJAP 38 (2S) (1999) 1094, http://dx.doi.org/10.1143/JJAP.38.1094.

[44] H. Kim, A. Murayama, J. Kim, J. Song, Temperature dependence of the radiative recombination time in laterally coupled GaAs quantum dots, Appl. Surf. Sci. 457 (2018) 497–500, http://dx.doi.org/10.1016/j.apsusc.2018.06.244.

[45] D. Gershoni, M. Katz, W. Wegscheider, L.N. Pfeiffer, R.A. Logan, K. West, Radiative lifetimes of excitons in quantum wires, Phys. Rev. B 50 (12) (1994) 8930–8933, http://dx.doi.org/10.1103/PhysRevB.50.8930.

[46] G. T. Hooft, M. Leys, H. Talen-v.d. Mheen, Temperature dependence of the radiative recombination coefficient in GaAs(Al, Ga)As quantum wells, Superlattices Microstruct. 1 (4) (1985) 307–310, http://dx.doi.org/10.1016/0749-6036(85)90092-8.

[47] R. Butkutė, V. Pačebutas, A. Krotkus, N. Knaub, K. Volz, Migration-enhanced epitaxy of thin GaAsBi layers, Lith. J. Phys. 54 (2) (2014) 125–129, http://dx.doi.org/10.3952/physics.v54i2.2922.

[48] R. Butkutė, M. Skapas, A. Selskis, V. Bukauskas, S. Stanionytė, G. Niaura, AlAs as a Bi blocking barrier in GaAsBi multi-quantum wells: Structural analysis, Lith. J. Phys. 57 (1) (2017) 29–36, http://dx.doi.org/10.3952/physics.v57i1.3453.

[49] Y. Horikoshi, Migration-enhanced epitaxy of GaAs and AlGaAs, Semicond. Sci. Technol. 8 (6) (1993) 1032–1051, http://dx.doi.org/10.1088/0268-1242/8/6/010.

[50] Y. Horikoshi, M. Kawashima, H. Yamaguchi, Migration-enhanced epitaxy of GaAs and AlGaAs, Japan. J. Appl. Phys. 27 (2R) (1988) 169, http://dx.doi.org/10.1143/JJAP.27.169.